The 9th European Congress on Computational Methods in Applied Sciences and Engineering
ECCOMAS Congress 2024
3 – 7 June 2024, Lisboa, Portugal

ADAPTIVE REFINEMENT TECHNIQUES USING MULTIRESOLUTION WAVE PROPAGATION SIMULATIONS GUIDED BY INHERENT CONVERGENCE INDICATORS

DIMITRIS K. DIMITRIOU, AIKATERINI B. SAMARA AND DIMITRIS A. SARAVANOS

Dept. of Mechanical Engineering and Aeronautics
University of Patras
Patras University Campus, Patras, Greece, GR-26504
e-mail: d.dimitriou@ac.upatras.gr

Key words: Multiresolution analysis, Convergence indicators, Wave propagation, Adaptive refinement, Daubechies wavelets.

Summary. The multiresolution finite wavelet domain method has been meticulously studied in wave propagation simulations. The multiresolution procedure always starts with the coarse solution, and then finer solutions can be superimposed on the coarse solution, until convergence is achieved. Based on remarkable observations on the multiple resolution components of the method, a residual-based convergence indicator that reveals convergence at the coarse solution is developed. This convergence metric is rapidly applicable and straightforward and can also divulge the spatial and temporal ranges/domains that the already obtained solution needs to be enhanced. In that way, an automatic adaptive refinement technique is proposed for the local enrichment of the solution, only in the specific grid points and time-steps that it is needed. A numerical case study regarding wave propagation in an inhomogeneous rod manifests the effectiveness and accuracy of the proposed automatic refinement methodology, as also the performance of the suggested convergence indicator.

1 INTRODUCTION

In many domains of physical research and engineering, the combination of wavelets and computer techniques seems to be incredibly effective and potent. Wavelet functions [1], [2] are attractive as basis functions in numerical methods [3], [4] because of their exceptional mathematical features. As such, numerous multiresolution wavelet-based techniques have been developed in recent years. A wavelet multiresolution interpolation Galerkin method (WMIGM) for nonlinear boundary value problems (BVPs) was constructed by Liu et al. [5]. Their approach showed excellent accuracy and stability results. Wang et al. [6] developed a multiresolution wavelet-based method for bending problems of complex-shaped plate structures. Their method outperformed conventional finite element (FE) models in terms of accuracy and efficiency. Also, Harten introduced a multiresolution approach that can hierarchically refine the solution of hyperbolic conservation laws [7]. Using second-generation wavelets, Azdoud and Ghosh [8] introduced an adaptive wavelet-enriched hierarchical finite element method. Their method was employed to solve static analyses of microstructures with polycrystals. With the use of phase-

field modeling, Cheng, Tu, and Ghosh [9] extended this technique to simulate the propagation of cracks in polycrystalline microstructures and found excellent convergence characteristics. For the effective study of shock waves, Gusto and Plewa [10] suggested a hybrid adaptive multiresolution method. Kaiser et al. [11] demonstrated excellent outcomes by proposing an adaptive wavelet-based approach for the multiscale study of 1D static interface and interphase issues. Asymmetrical wavelets were used by Yang et al. [12] to create high-order adaptive multiresolution collocation techniques for the solution of hyperbolic conservation laws involving upwind schemes. Their technique proved to be highly effective and precise when analyzing 1D shock turbulence interaction problems and interacting blast wave problems.

Most of the previously mentioned works are focused on the domain of computational fluid dynamics (CFD). Furthermore, all of the works previously mentioned specify the refinement domain of each problem using arbitrary threshold parameters. This fact diminishes the robustness and usefulness of adaptive approaches. In this work, a robust and straight-forward convergence indicator (CI) is proposed and used to estimate the refinement domain. This CI is based on the intrinsic characteristics of the multiresolution finite wavelet domain method (MR-FWD) that has been recently developed and utilized in transient dynamic simulations of rods, beams and 2D solids[13]–[15]. By employing the proposed convergence indicator, an automatic adaptive refinement methodology is presented for the efficient wave propagation simulation in rod structures, manifesting remarkable accuracy and computational gains.

2 THEORETICAL BACKGROUND

2.1 The multiresolution finite wavelet domain method

In the present section, the formulation of the MR-FWD method and the multiresolution hierarchical procedure are concisely presented. For more information, the reader can refer to [14], [16]. In **Figure 1,** a beam structure that is divided into 9 segments, using a uniform grid of 10 nodes, is portrayed. Additional 2L-2 grid points, where L is the order of Daubechies (DB) scaling function (SF) and wavelet function (WF), are introduced to the left side of the physical domain, forming the wavelet domain. The generalized displacement approximation in the segment between 2 grid points for *R* resolutions is expressed as:

$$u(x,t) = \sum_{n=2-2L}^{0} \hat{u}_{Cn}^{0}(t)\varphi(\xi - n) + \sum_{S=0}^{R}\{\sum_{n=2-2L}^{0} \hat{u}_{Fn}^{S}(t)\psi(2^{s}\xi - n)\} \tag{1}$$

where $\hat{u}_{Cn}^{0}$ are the coarse coefficients at resolution 0, $\hat{u}_{Fn}^{S}$ are the fine coefficients at resolution *S*, $\varphi(x)$ is the scaling function and $\psi(x)$ is the wavelet function. In the Appendix, the mathematical properties of Daubechies SFs and WFs are briefly mentioned. A normalized local coordinate system is associated with each element. The local dimensionless coordinate variable ξ is given as $\xi = (x - x_i)/(x_{i+1} - x_i) = (x - x_i)/l_e$ so, in Eq. (1) the spatial variables x and ξ are limited to the ranges $0 \le x \le l_e$ and $0 \le \xi \le 1$, respectively, where l_e is the elemental length. It is clear from **Figure 1** that the MR procedure starts with the coarse solution C^0 that only employs the SFs, and then that solution is incrementally enriched by the fine solutions of each resolution that utilize the WFs. The schematic representation of the 1D MR analysis (**Figure 1**) is analytically expressed in Eq. (1) for the generalized displacement field u. For simplicity, the MR process up to resolution 1 is presented in Eqs. (2) and (3).

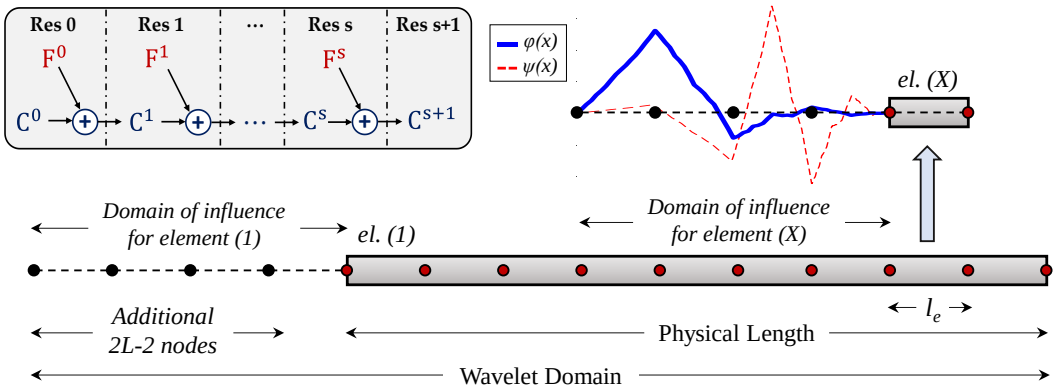

Figure 1: Representation of the 1D MR synthesis process and discretization style of the physical domain using nine DB3 wavelet-based "elements". The physical and wavelet domain are depicted.

Single-Resolution - Resolution 0 (C^0). The C^0 solution is obtained by utilizing only the DB SF, $\varphi(x)$, and provides the initial approximation for the MR process. The equation of motion is:

$$[\mathbf{M_{CC}}]\ddot{\hat{u}}^0_{CC} + [\mathbf{K_{CC}}]\hat{u}^0_{CC} = F_C \tag{2}$$

where $\hat{u}_{CC}$ are the generalized coarse coefficients of the SR approximation, $[\mathbf{K_{CC}}]$ and $[\mathbf{M_{CC}}]$ are the coarse resolution stiffness and mass matrices, and F_C is the coarse resolution load vector.

MR - Resolution 1 (C^1). Pursuing the MR reconstruction process, the fine approximation at resolution 0 (F^0) needs to be calculated and then added to the coarse solution at resolution 0 (C^0) so as to acquire the C^1 solution. The MR solution system is:

$$\begin{bmatrix} \mathbf{M_{CC}} & \mathbf{0} \\ \mathbf{0} & \mathbf{M_{FF}} \end{bmatrix} \begin{Bmatrix} \ddot{\hat{u}}^0_C \\ \ddot{\hat{u}}^0_F \end{Bmatrix} + \begin{bmatrix} \mathbf{K_{CC}} & \mathbf{K_{CF}} \\ \mathbf{K_{FC}} & \mathbf{K_{FF}} \end{bmatrix} \begin{Bmatrix} \hat{u}^0_C \\ \hat{u}^0_F \end{Bmatrix} = \begin{Bmatrix} F_C \\ F_F \end{Bmatrix} \tag{3}$$

where $\hat{u}_F$ are the generalized fine coefficients and $\hat{u}_C$ are the generalized coarse coefficients of the coupled equations of motion for resolution 1. It should be highlighted that $\hat{u}_C$ is not equal to $\hat{u}_{CC}$ because of the stiffness coupling terms, $[\mathbf{K_{CF}}]$ and $[\mathbf{K_{FC}}]$, once the first derivatives of $\varphi(x)$ and $\psi(x)$ are not cross-orthogonal. Also, $[\mathbf{K_{FF}}]$ and $[\mathbf{M_{FF}}]$ are the fine resolution stiffness and mass matrices, respectively, and F_F is the fine resolution load vector.

Hierarchical procedure – Explicit integration. Following the MR reconstruction approach, the first step of the process is always the single-resolution coarse component. The MR procedure will be described for resolution 1. The coarse component at resolution 0, $\hat{u}^0_{CC}$, is already calculated. The component $\hat{u}^0_C$ of resolution 0, is set as $\hat{u}^0_C = \Delta\hat{u}^0 + \hat{u}^0_{CC}$, where $\Delta\hat{u}^0$ is termed as correction component. In that way, Eq. (3) can be written as:

$$\begin{bmatrix} \mathbf{M_{CC}} & 0 \\ 0 & \mathbf{M_{FF}} \end{bmatrix} \begin{Bmatrix} \Delta\ddot{\hat{u}}^{0,t} \\ \ddot{\hat{u}}_F^{0,t} \end{Bmatrix} + \begin{bmatrix} \mathbf{K_{CC}} & \mathbf{K_{CF}} \\ \mathbf{K_{FC}} & \mathbf{K_{FF}} \end{bmatrix} \begin{Bmatrix} \Delta\hat{u}^{0,t} \\ \hat{u}_F^{0,t} \end{Bmatrix} = \begin{Bmatrix} 0 \\ F_F^t - \mathbf{K_{FC}}\hat{u}_{CC}^{0,t} \end{Bmatrix} \tag{4}$$

Using central differences, the three forenamed components at resolution 0 are calculated as:

$$\hat{u}_{CC}^{0,t+1} = \left(a_0\mathbf{M_{CC}}\right)^{-1}\left(F_C^t + \mathbf{M_{CC}}\left(2a_0\hat{u}_{CC}^{0,t} - a_0\hat{u}_{CC}^{0,t-1}\right) - \mathbf{K_{CC}}\hat{u}_{CC}^{0,t}\right) \tag{5}$$

$$\Delta\hat{u}^{0,t+1} = \left(a_0\mathbf{M_{CC}}\right)^{-1}\left(\mathbf{M_{CC}}\left(2a_0\Delta\hat{u}^{0,t} - a_0\Delta\hat{u}^{0,t-1}\right) - \mathbf{K_{CC}}\Delta\hat{u}^{0,t} - \mathbf{K_{CF}}\hat{u}_F^{0,t}\right) \tag{6}$$

$$\hat{u}_F^{0,t+1} = \left(a_0\mathbf{M_{FF}}\right)^{-1}\left(F_F^t + \mathbf{M_{FF}}\left(2a_0\hat{u}_F^{0,t} - a_0\hat{u}_F^{0,t-1}\right) - \mathbf{K_{FC}}\left(\hat{u}_{CC}^{0,t} + \Delta\hat{u}^{0,t}\right) - \mathbf{K_{FF}}\hat{u}_F^{0,t}\right) \tag{7}$$

where $a_0 = 1/\Delta t^2$ and Δt is the time step for the explicit integration scheme. The summation of the three forenamed components at resolution 0, forms the coarse approximation of the next resolution (resolution 1), as:

$$\hat{u}_{CC}^1 = \hat{u}_{CC}^0 + \Delta\hat{u}^0 + \hat{u}_F^0 \tag{8}$$

3 CONVERGENCE INDICATOR & ADAPTIVE REFINEMENT

3.1 Residual-based Convergence Indicator

In this section it is shown that the maximum ratio of the uncoupled fine solution to the coarse one basically constitutes a convergence indicator (CI) that reveals convergence at resolution 1. The uncoupled fine solution, $\hat{u}_F^{unc}$, is determined as:

$$\hat{u}_F^{unc} = \left[\mathbf{K_{FF}}\right]^{-1}\mathscr{R} \tag{9}$$

where the term $\mathscr{R} = F_F - [\mathbf{K_{FC}}]\hat{u}_{CC}^0$ is called the Residual vector. The uncoupled fine solution is basically the fine solution that can be calculated by ignoring the correction component. Also, the inertial terms have been ignored since the dynamic characteristics of the solution are provided by the coarse component. In this way, the computation of the uncoupled fine solution is rapid since time integration is not needed. The refinement region (Ω) for resolution 1 can be estimated through the proposed indicator for resolution 0:

$$\Omega : CI_{1D}^R = \max\frac{\left|u_F^{unc}\right|}{\left|u_{CC}^0\right|} > \varepsilon \tag{10}$$

where ε is a critical threshold value that depends on the order of Daubechies wavelet family and is estimated from convergence studies, as shown hereafter. Convergence studies using the DB3 SFs/WFs for the wavelet-based elements were carried out for 4 rods with different Elastic Modulus. All the other material and geometric characteristics are exactly the same, namely, the rod's length is $l=4m$ and cross section $A=10^{-4}m^2$, Poisson's ratio $v=0.3$, density $\rho=2700\ kg/m^3$, clamped at its left side and excited at its center with a 5-cycle tone burst with 25 kHz central

frequency. In **Figure 2a** the values of the CIs for each material case and different discretizations are shown. As anticipated, the lines differ from each other since the different material changes the dynamic behavior and so, different number of nodes leads to different ratios of uncoupled fine to coarse solution. Interestingly, in the plot of RMS errors vs the CIs (**Figure 2b**), all the lines coincide. This is very important since it seems that the proposed convergence indices are material-invariant and robust. Also, the behavior of those indicators is monotonous, and notably, the CI values are monotonically decreasing with the decrease of the RMS error. This means that a threshold value can be selected for a given RMS error where the analysis results are considered as accurate. The threshold value for this study will be set as $\varepsilon=0.01$ for the DB3 elements. It is highlighted that the material-invariant behavior and monotonicity of the proposed CI has been checked in numerous cases that are not presented for the sake of brevity.

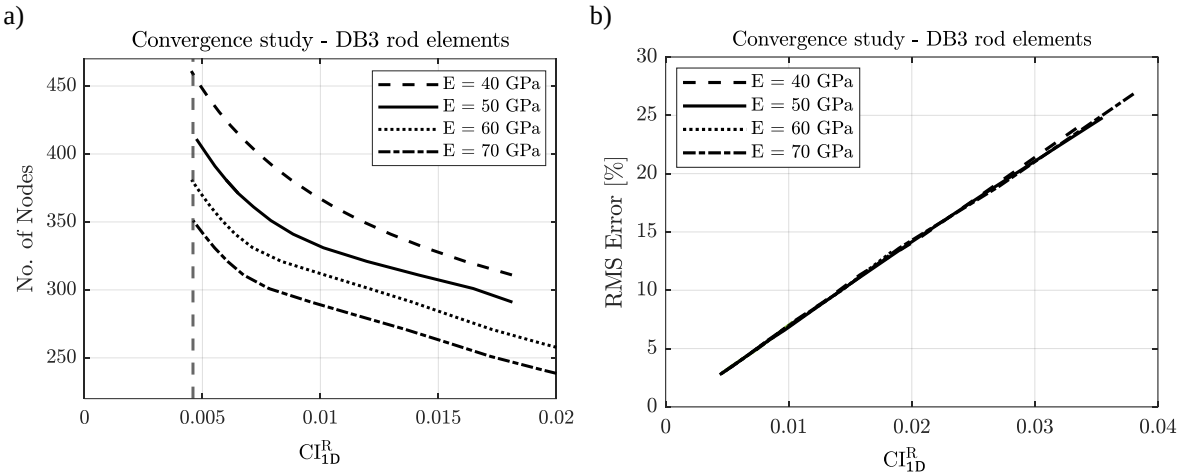

Figure 2: Convergence indicator values (a) versus no. of nodes, and (b) versus RMS error, for 4 different material cases.

For the demonstration of the uncoupled fine solution and the respective convergence index, the following case study is shown: an inhomogeneous rod with length $l=4m$ and cross section $A=10^{-4}m^2$ is modeled. The rod consists of two different materials, aluminum, and damaged aluminum, and their mechanical properties are shown in Table 1. The damage or compliant material spans from $0m \leq x \leq 2m$ (**Figure 3**). The rod is clamped at the left edge, and it is axially excited at its center ($x=2m$) by a 5-cycle tone burst with 25 kHz central frequency. The analysis duration is 0.4 ms and the model uses 120 DB6 wavelet-based elements.

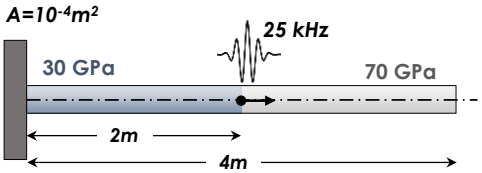

Figure 3: Geometric representation of an inhomogeneous rod structure.

It is shown that the coarse solution exhibits different wavenumbers and group velocities at its left and right half when it comes to the spatial axis (**Figure 4a**). This is expected due to the different material. Specifically, the left half ($0m \leq x \leq 2m$) reveals higher wavenumbers and lower

group velocity than the right half because of the more compliant material. The fine uncoupled solution (**Figure 4b**) qualitatively acts like the fine solution by basically isolating the damage span. Due to that filter behavior, the proposed CI (**Figure 4c**) suggests that the part of the solution that needs to be enriched is the wave packet that travels in the damaged region while accurately specifying its limits in both space and time.

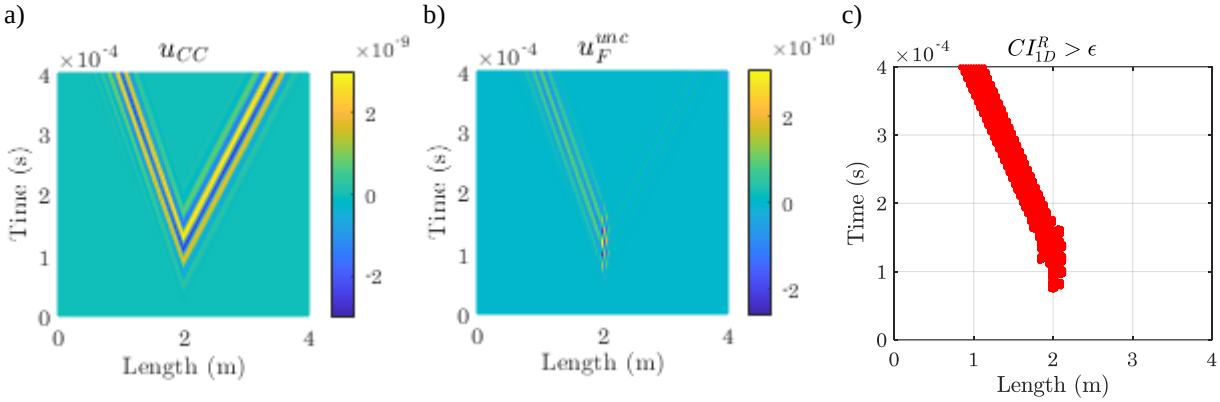

Figure 4: Coarse solution (a), uncoupled fine solution (b) and the respective convergence indicator (c) that designates the refinement domain.

3.2 Adaptive Refinement

As already mentioned, the C^0 solution is always calculated for the whole spatial and temporal domain. After obtaining the C^0 solution and calculating the indicator that specifies the domain that needs refinement, the resolution 1 components can be computed only where needed. The components using adaptive refinement are expressed as:

$$\Delta\hat{u}^{0,r,t+1} = \left(a_0\mathbf{M}^{\mathbf{r}}_{\mathbf{CC}}\right)^{-1}\left(\mathbf{M}^{\mathbf{r}}_{\mathbf{CC}}\left(2a_0\Delta\hat{u}^{0,r,t} - a_0\Delta\hat{u}^{0,r,t-1}\right) - \mathbf{K}^{\mathbf{r}}_{\mathbf{CC}}\Delta\hat{u}^{0,r,t} - \mathbf{K}^{\mathbf{r}}_{\mathbf{CF}}\hat{u}^{0,r,t}_F\right) \quad (11)$$

$$\hat{u}^{0,r,t+1}_F = \left(a_0\mathbf{M}^{\mathbf{r}}_{\mathbf{FF}}\right)^{-1}\left(\mathbf{M}^{\mathbf{r}}_{\mathbf{FF}}\left(2a_0\hat{u}^{0,r,t}_F - a_0\hat{u}^{0,r,t-1}_F\right) - \mathbf{K}^{\mathbf{r}}_{\mathbf{FC}}\left(\hat{u}^{0,r,t}_{CC} + \Delta\hat{u}^{0,r,t}\right) - \mathbf{K}^{\mathbf{r}}_{\mathbf{FF}}\hat{u}^{0,r,t}_F\right) \quad (12)$$

where the superscript r denotes the refinement domain. That means that those vectors and matrices are only calculated in a much smaller domain than the initial one, reducing the system's size. The refined prediction at resolution 1 is:

$$\hat{u}^{1,r}_{CC} = \hat{u}^{0}_{CC} + \Delta\hat{u}^{0,r} + \hat{u}^{0,r}_F \quad (13)$$

4 NUMERICAL CASE STUDY

In this subsection, the automatic adaptive refinement process is presented in a case study of wave propagation in an inhomogeneous rod structure. In **Figure 5a**, an inhomogeneous rod with length $l=7m$ and cross section $A=10^{-4}m^2$ is illustrated, that is comprised of two different materials, shown in Table 1. The light grey is the Aluminum part while the dark grey is the Damaged Aluminum part. The rod is clamped at its left side and is axially excited at its center by a 5-cycle tone burst with 25 kHz central frequency.

Table 1: Material properties.

	E (GPa)	v	ρ (kg/m^3)
Aluminum	70	0.3	2700
Damaged Aluminum	30	0.3	2700

In **Figure 5b,c**, the spatiotemporal response of the coarse and uncoupled fine solution is depicted, respectivelly, and in **Figure 5d** the adaptive refinement domain that is automatically derived from the forenamed CI is displayed. Its demonstrated that the solution needs enrichment inside the damaged area, and also on the transmitted wave at the right of the damage span.

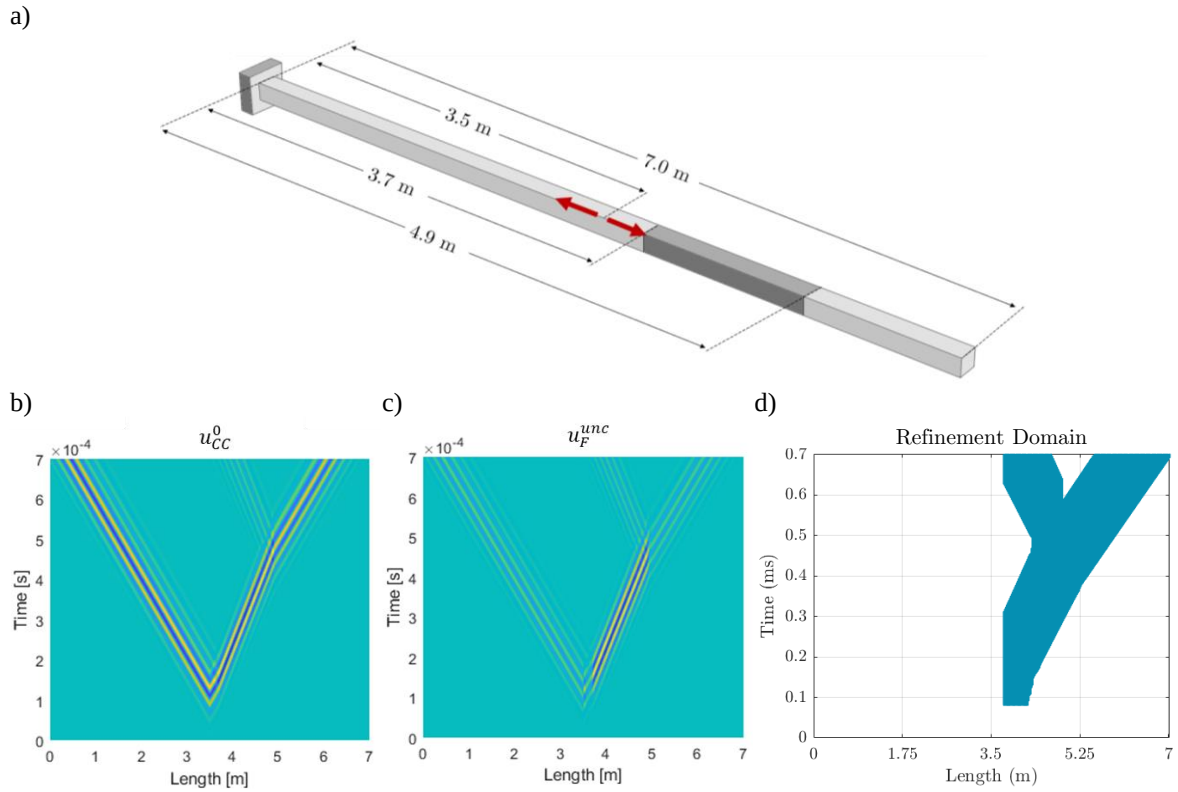

Figure 5: (a) Illustration of the inhomogeneous rod, (b) spatiotemporal plot of the coarse solution, (c) spatiotemporal plot of the uncoupled fine solution and (d) visualization of the adaptive refinement domain.

It is observed in **Figure 6** that the coarse solution exhibits substantial error compared to the full domain MR solution. The full domain MR solution is the classic C^1 solution that is calculated in the whole spatiotemporal domain. The targeted MR solution is calculated at two different spans of the rod, as shown by the refinement regions in **Figure 6**, and is accurate as it coincides with the full domain solution. It should be highlighted that this procedure is fully automated since the CI is rapidly computed and guides the adaptive refinement technique.

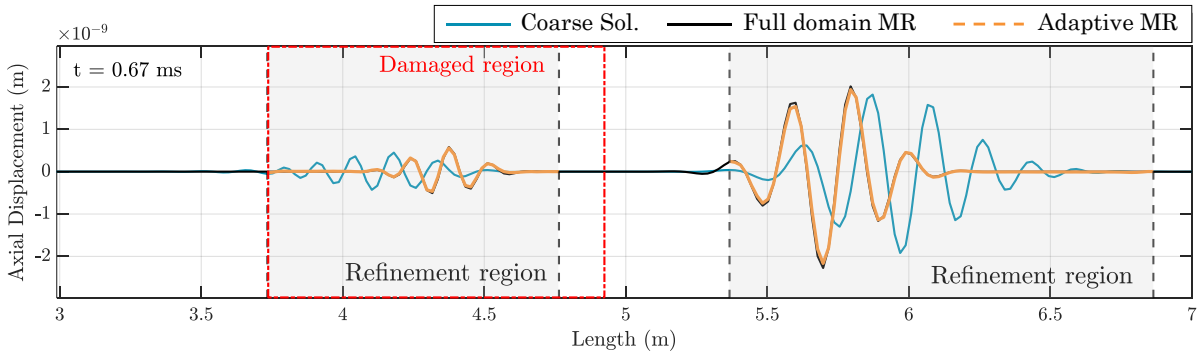

Figure 6: Axial displacements for each solution at t=0.67 ms.

Concerning the computational gains, the adaptive MR refinement solution is expected to be faster than the full domain MR solution since the Eqs. (11), (12) are solved for fewer time steps and have smaller algebraic size. This is of course problem-dependent and is affected by the size of the refinement domain in space and time. For the already presented numerical example, the adaptive MR refinement is about 10 times faster than the full domain MR refinement, as illustrated in **Figure 7a**. As already mentioned, the coarse solution (C^0) is always calculated in the whole spatiotemporal domain, as provided in Eq. (5). That is why the blue coloured bar that indicates the solver duration of resolution 0 solution (C^0) is the same for the full domain and the adaptive MR solution. However, the calculation of Eqs. (6), (7) at the whole spatiotemporal domain for the full domain MR solution is 10 times slower than the calculation of Eqs. (11), (12) for the adaptive MR solution, as suggested by the red coloured bars in **Figure 7a**. The overall adaptive MR solution is 2.3 times faster than the full domain MR solution for this specific case study. In **Figure 7b**, the normalized solver durations of different converged FE and wavelet-based models are compared. The proposed adaptive MR solution is about 15 times faster than the single-resolution (SR) solution and about 55 and 460 times faster than 3-node and 2-node FE models, respectivelly. Finally, it should be mentioned that the RAM requirements are also crucially decreased using the proposed adaptive methodology.

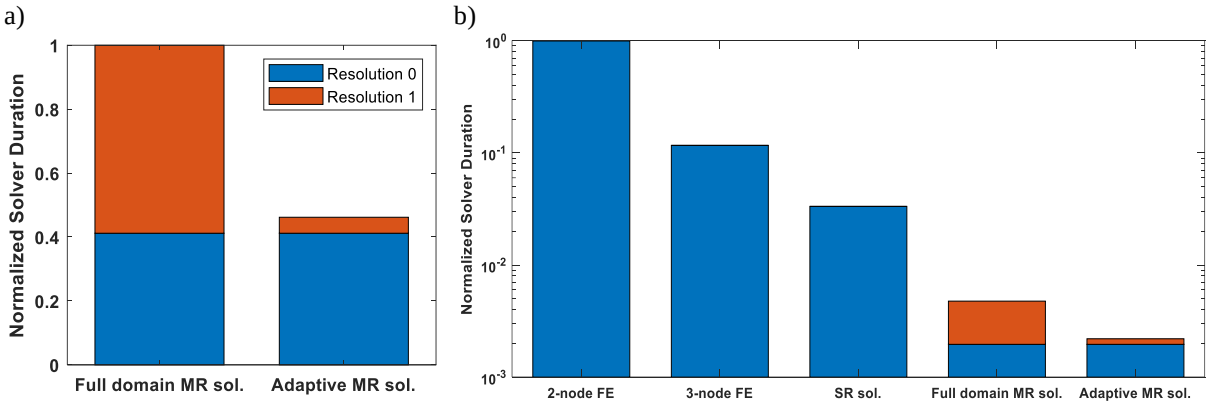

Figure 7: Normalized solver durations of (a) full domain vs adaptive MR solution and (b) different finite element and wavelet-based models.

5 CONCLUSIONS

In this work, an automatic adaptive refinement technique is introduced, based on the inherent convergence indicators provided by the MR-FWD method. The robustness of the proposed residual-based convergence indicator is shown, and its great performance is validated towards the numerical simulation of wave propagation in an inhomogeneous rod. The convergence indicator successfully specifies the domain that the initial solution needs to be enhanced, leading to a very accurate and efficient automatic methodology. The computational gains of the presented methodology in terms of CPU times are also quantified, manifesting up to 460 times faster simulations compared to traditional finite element models.

ACKNOWLEDGMENTS

The research work was supported by the Hellenic Foundation for Research and Innovation (HFRI) under the 3rd Call for HFRI PhD Fellowships (Fellowship Number: 5509).

REFERENCES

[1] Y. Meyer, *Wavelets and Operators*. Cambridge, UK: Cambridge University Press, 1992.

[2] S. G. Mallat, *A Wavelet Tour of Signal Processing*, 3rd editio. Elsevier, 2010.

[3] B. Li and X. Chen, "Wavelet-based numerical analysis: A review and classification," *Finite Elem. Anal. Des.*, vol. 81, pp. 14–31, 2014, doi: 10.1016/j.finel.2013.11.001.

[4] J. Wang, X. Liu, and Y. Zhou, "Application of Wavelet Methods in Computational Physics," *Ann. Phys.*, vol. n/a, no. n/a, p. 2300461, 2024, doi: https://doi.org/10.1002/andp.202300461.

[5] X. Liu, Y. Zhou, and J. Wang, "Wavelet multiresolution interpolation Galerkin method for nonlinear boundary value problems with localized steep gradients," *Appl. Math. Mech.*, vol. 43, no. 6, pp. 863–882, 2022, doi: 10.1007/s10483-022-2859-5.

[6] Y. Z. Jizeng WANG, Yonggu FENG, Cong XU, Xiaojing LIU, "Multiresolution method for bending of plates with complex shapes," *Appl. Math. Mech. (English Ed.*, vol. 44, no. 11925204, pp. 561–582, 2023, doi: https://doi.org/10.1007/s10483-023-2972-8.

[7] A. Harten, "Multiresolution algorithms for the numerical solution of hyperbolic conservation laws," *Commun. Pure Appl. Math.*, vol. 48, no. 12, pp. 1305–1342, 1995, doi: 10.1002/cpa.3160481201.

[8] Y. Azdoud and S. Ghosh, "Adaptive wavelet-enriched hierarchical finite element model for polycrystalline microstructures," *Comput. Methods Appl. Mech. Eng.*, vol. 321, pp. 337–360, 2017, doi: 10.1016/j.cma.2017.04.018.

[9] J. Cheng, X. Tu, and S. Ghosh, "Wavelet-enriched adaptive hierarchical FE model for coupled crystal plasticity-phase field modeling of crack propagation in polycrystalline microstructures," *Comput. Methods Appl. Mech. Eng.*, vol. 361, p. 112757, 2020, doi: 10.1016/j.cma.2019.112757.

[10] B. Gusto and T. Plewa, "A hybrid adaptive multiresolution approach for the efficient simulation of reactive flows," *Comput. Phys. Commun.*, vol. 274, 2022, doi: 10.1016/j.cpc.2022.108300.

[11] T. Kaiser, J. J. C. Remmers, and M. G. D. Geers, "An adaptive wavelet-based collocation

method for solving multiscale problems in continuum mechanics," *Comput. Mech.*, vol. 70, no. 6, pp. 1335–1357, 2022, doi: 10.1007/s00466-022-02207-5.

[12] B. Yang, J. Wang, X. Liu, and Y. Zhou, "High-order adaptive multiresolution wavelet upwind schemes for hyperbolic conservation laws," *Comput. Fluids*, vol. 269, no. September 2023, p. 106111, 2024, doi: 10.1016/j.compfluid.2023.106111.

[13] C. V. Nastos and D. A. Saravanos, "Multiresolution Daubechies finite wavelet domain method for transient dynamic wave analysis in elastic solids," *Int. J. Numer. Methods Eng.*, vol. 122, no. 23, pp. 7078–7100, 2021, doi: 10.1002/nme.6822.

[14] D. K. Dimitriou, C. V Nastos, and D. A. Saravanos, "Multiresolution finite wavelet domain method for efficient modeling of guided waves in composite beams," *Wave Motion*, vol. 112, p. 102958, 2022, doi: https://doi.org/10.1016/j.wavemoti.2022.102958.

[15] D. K. Dimitriou, C. V Nastos, and D. A. Saravanos, "A multiresolution layerwise method with intrinsic damage detection capabilities for the simulation of guided waves in composite strips," *J. Vib. Control*, Mar. 2023, doi: 10.1177/10775463231158667.

[16] C. V. Nastos and D. A. Saravanos, "Multiresolution Daubechies Finite Wavelet Domain Method for Transient Dynamic Wave Analysis in Elastic Solids," *Int. J. Numer. Methods Eng.*, pp. 1–37, 2021, doi: 10.1002/nme.6822.

[17] I. Daubechies, *Ten Lectures on Wavelets*. SIAM, 1992.

APPENDIX

Mathematical properties of Daubechies wavelets

The Daubechies wavelet family consists of compactly supported scaling functions $\varphi(x)$ and wavelet functions $\psi(x)$ [17]. Their basic mathematical properties are:

Compact Support. Both SFs and WFs are bounded within an interval, which spans over a compact support domain of grid points [0, 2L − 1], where L is the order of the SF/WF. Hereafter, DB SFs/WFs of order L are termed as DBL.

Orthogonality. The integer translates of the SFs/WFs are orthogonal to each other, so they form an orthogonal basis in the Lebesgue space,

$$\int_{-\infty}^{\infty} \varphi(x-i)\varphi(x-j)dx = \delta_{ij}, \int_{-\infty}^{\infty} \psi(x-i)\psi(x-j)dx = \delta_{ij}, \int_{-\infty}^{\infty} \varphi(x-i)\psi(x-j) = 0 \qquad (14)$$

Vanishing moments. The number of vanishing moments signifies the maximum degree of polynomial that can be exactly approximated by SF/WF. DB SFs/WFs of order L have L vanishing moments and can exactly represent polynomials up to L-1 order.

Two scale relation/ Dilation property. The dilation property constitutes the basis for the MR analysis. It is provided by the dilation equations,

$$\varphi(2^j x) = \sqrt{2} \cdot \sum_{k=0}^{2L-1} h_k \cdot \varphi(2^{j+1}x - k), \qquad \psi(2^j x) = \sqrt{2} \sum_{k=0}^{2L-1} (-1)^k h_{2L-k-1} \cdot \varphi(2^{j+1}x - k) \quad (15)$$

where h_k is the set of 2L filter coefficients, and j is the resolution or scale.